Acta Materialia 176 (2019) 297–305

Contents lists available at ScienceDirect

Acta Materialia

journal homepage: www.elsevier.com/locate/actamat

Metallic glasses for biodegradable implants

Denise C. Ford [a], David Hicks [a], Corey Oses [a], Cormac Toher [a], Stefano Curtarolo [a, b, *]

[a] Department of Mechanical Engineering and Materials Science and Center for Materials Genomics, Duke University, Durham, NC, 27708, USA
[b] Department of Electrical Engineering, Physics and Chemistry, Duke University, Durham, NC, 27708, USA

ARTICLE INFO

Article history:
Received 30 April 2019
Received in revised form
1 July 2019
Accepted 3 July 2019
Available online 6 July 2019

Keywords:
Bulk metallic glass
Biodegradable implant
Orthopedic
Computational materials
High-throughput calculations

ABSTRACT

Metallic glasses are excellent candidates for biomedical implant applications due to their inherent strength and corrosion resistance. However, use of metallic glasses in structural applications is limited because bulk dimensions are challenging to achieve. Glass-forming ability (GFA) varies strongly with alloy composition and becomes more difficult to predict as the number of chemical species in a system increases. Here, we present a theoretical model — implemented in the AFLOW framework — for predicting GFA based on the competition between crystalline phases. The model is applied to biologically relevant binary and ternary systems. Elastic properties of Ca- and Mg-based systems are estimated for use in biodegradable orthopedic support applications. Alloys based on $Ag_{0.33}Mg_{0.67}$, $Cu_{0.5}Mg_{0.5}$, $Cu_{0.37}Mg_{0.63}$, and $Cu_{0.25}Mg_{0.5}Zn_{0.25}$, and in the Ag-Ca-Mg and Ag-Mg-Zn systems, are recommended for further study.

© 2019 Acta Materialia Inc. Published by Elsevier Ltd. All rights reserved.

1. Introduction

Metallic glasses demonstrate greater strength and corrosion resistance than their crystalline counterparts, and are therefore highly sought-after materials for a variety of applications, such as precision gears, sporting goods, and medical devices [1–5]. These properties are of particular importance for biomedical implant applications, as implant materials must maintain function and biocompatibility in a chemically and mechanically complex physiological environment. For example, stainless steel — well-known for strength, corrosion resistance, and biocompatibility — is commonly used in implantable devices (*e.g.* vascular stents, pacemakers, and total joint replacements) [6]. However, materials-related failure of these devices does occur and can necessitate a revision surgery. In particular, structural support implants are plagued by fatigue and stress corrosion cracking, despite optimization of the steel by alloying and surface treatments [6]. Ions are released during corrosion and structural failure, which can lead to allergic reaction, metallosis, or toxicity.

An intentionally degradable material can be used for applications where only temporary support is required, such as bone plates and coronary stents. This reduces the occurrence of implant removal surgeries and eliminates concern over long-term embedding of a foreign object. Mg-based alloys are considered for orthopedic applications: densities and mechanical properties are similar to bone, and Mg is an essential nutrient for humans that is active in bone development [7]. Despite favorable characteristics and intense study over the last two decades [8–12], Mg-based alloys are still not in wide-spread clinical use because they often degrade too quickly forming hydrogen gas. When the rate is too high, bubbles can interfere with tissue healing [13–16], block the blood stream, or cause alkaline poisoning [13,15].

Alternative to traditional metallurgical approaches — alloying and heat treating — strength and corrosion resistance can be improved for a material by forming an amorphous structure. Since glasses lack grain boundaries and dislocations, galvanic couples are reduced and slip planes are eliminated. Ion diffusion may be slowed by elimination of structural defects, enhancing corrosion resistance. Many studies indicate that metallic glasses have higher yield strength than their crystalline counterparts, and the yield strength increases with the glass transition temperature [17]. Fe-based metallic glasses have been shown to passivate/repassivate quickly in aqueous solutions and have high resistance to pitting, potentially retarding stress corrosion cracking [18]. No hydrogen evolution could be clinically observed for a Mg-Zn-Ca metallic glass studied for biomedical implant purposes [19]. Absence of structural defects can be problematic for support applications because plastic deformation cannot occur. Many metallic glasses have been shown to

* Corresponding author. Department of Mechanical Engineering and Materials Science and Center for Materials Genomics, Duke University, Durham, NC, 27708, USA.
E-mail address: stefano@duke.edu (S. Curtarolo).

https://doi.org/10.1016/j.actamat.2019.07.008
1359-6454/© 2019 Acta Materialia Inc. Published by Elsevier Ltd. All rights reserved.

undergo brittle fracture [17], and increasing ductility is an active research area [20,21].

Discovery of new metallic glass-forming systems has been vigorously pursued over the past few decades. The empirical rules devised by Inoue [22] have been heavily relied upon for experimental discovery. However, further guidance is needed. Recent estimates indicate that there are ~3 million potential binary, ternary, and quaternary bulk metallic glasses based on empirical rules [23]. Even with high-throughput combinatorial experimentation, it could take up to a decade to search the ternary space of 30 common elements in metallic glasses [24]. Physical models for glass-forming ability (GFA) have been suggested [25–28], yet no complete, robust theory exists. Recently, the concept of structural confusion during cooling advanced by Greer in 1993 [29] has been explored computationally by Perim et al. [30] with reasonable success. A glass-forming descriptor was devised based on the distribution of the formation enthalpies of compounds available in a given system (probability of occurrence) and the similarity between their crystal structures (large differences creating confusion). The descriptor was successfully applied to binary alloys in the AFLOW.org repository [31–33] of first-principles calculations. However, extension to higher-order systems is not trivial. Glass-forming ability is expected to increase with the number of species in a system because the configuration space grows [28], but this is not always the case [26,27]. Since the GFA of a glass directly relates to the critical dimensions of a glassy alloy, it is of great technological interest to predict materials with high GFA for use in applications where bulk dimensions are required.

Here, the concept of structural confusion in the prediction of GFA [29,30] is generalized to higher-order systems. In the remainder of this article, the formalism for the computation of GFA is defined and validated against known bulk glass-forming systems. Predictions are presented for glass-formation in biologically relevant binary and ternary alloy systems, and elastic properties for Ca- and Mg-based systems are estimated using the rule of mixtures. Finally, alloys are recommended for orthopedic support applications.

2. Methods

2.1. Calculation of glass-forming ability

The GFA calculation in Ref. [30] quantifies confusion by comparing all of the metastable structures available at a given stoichiometry vector, $\{X\}$, to a reference state — the structure with the lowest enthalpy of formation at $\{X\}$. An average structural similarity between metastable structures is also considered. Individual structures are represented by a vector, ψ_i, of the local atomic environments (AE) [34] calculated for each unique atom. The AE of an atom is defined as the polyhedron formed by the atoms within the maximum gap in the radial distribution function. Functions describing the similarity between the structures, difference between the formation enthalpy of a metastable structure, H_i, and the reference state, and sampling are combined as:

$$\chi_{\mathrm{GFA}}(\{X\}) = \frac{\sum_i f(|\psi_i\rangle) g(H_i)}{\#\ \text{structures}}. \tag{1}$$

This works well as a first-order approximation for binary systems. In real systems, however, local variations in composition introduce additional competition between structures with different stoichiometries. Including these contributions, along with a more accurate description of the reference state and system chemistry, improves the physicality of the model and applicability to higher-order systems.

Here, the GFA is calculated at the global stoichiometry, $\{X\}$, and contains contributions from structures with (local) stoichiometries, $\{x\}$. Linear combinations, designated as pseudostructure ϕ_l with stoichiometry $\{X\}_l$, are created from structures ψ_i with stoichiometry $\{x\}_i$. Coefficients, $b_{l,i}$, are assigned to balance the local stoichiometries with the global stoichiometry:

$$\sum_i b_{l,i}\{x\}_i = \{X\}_l. \tag{2}$$

The concept is depicted in Fig. 1. The AE (denoted AE_α) is calculated for each unique atom in each ψ_i, and carries a coefficient, $c_{l,\alpha}$. This coefficient accounts for number of times AE_α occurs in ψ_i, $N_{i,\alpha}$, weighted by the amount of ψ_i present in ϕ_l, $b_{l,i}$. Mathematically, the combination is written as:

$$|\phi_l\rangle = \sum_\alpha c_{l,\alpha}|AE_\alpha\rangle, \qquad \langle AE_\alpha|AE_\beta\rangle = \delta_{\alpha\beta},$$
$$\sum_\alpha c_{l,\alpha}^2 = 1, \qquad c_{l,\alpha} = \frac{\sum_i b_{l,i}N_{i,\alpha}}{\sqrt{\sum_\alpha\left(\sum_i b_{l,i}N_{i,\alpha}\right)^2}}, \tag{3}$$

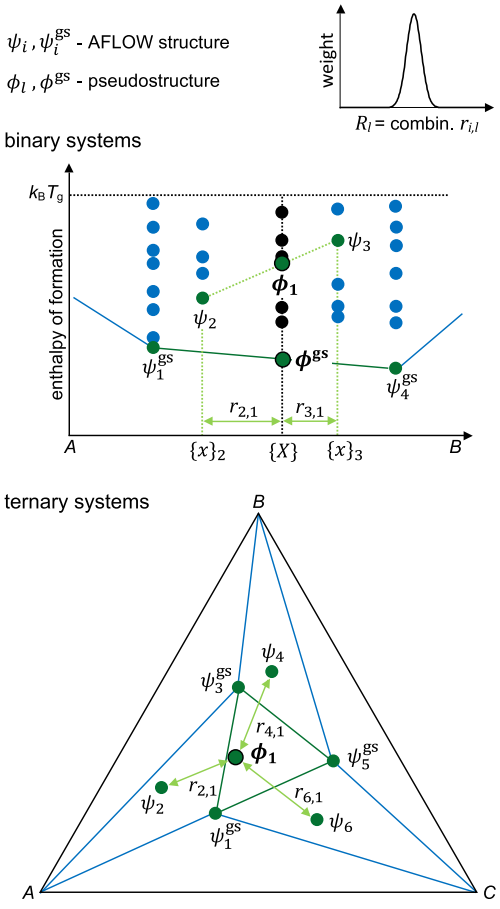

Fig. 1. Schematic of contributions to the GFA. Structures are represented as circles: black are at the global stoichiometry, blue are at other stoichiometries, and green highlight contributing pairs and triplets. Pseudostructures are represented as green circles outlined in black. The reference state is the ground state (gs) defined by the convex hull. In the ternary schematic, ϕ^{gs} is located directly beneath ϕ_1. The cutoff energy for including structures in the analysis is based on a typical glass transition temperature, T_g. The weight of each contributing pair (triplet) is taken from a Gaussian distribution. (For interpretation of the references to colour in this figure legend, the reader is referred to the Web version of this article.)

where $\delta_{\alpha\beta}$ is the Kronecker δ. Linear combinations of pairs and triplets are created for binary and ternary alloy systems, respectively. A cutoff energy — set to a typical glass transition temperature, T_g, times the Boltzmann constant, k_B — is imposed for including structures in the analysis.

The reference state at $\{X\}$ is the ground state defined by the convex hull, which is calculated using AFLOW-CHULL [35]. It may consist of one or more structures (decomposition products). Therefore, it is represented as a pseudostructure, ϕ^{gs}, and defined in the same way as Eqn. (3).

The similarity between two pseudostructures, ϕ_l and ϕ_m, is quantified by the scalar product:

$$\langle \phi_l | \phi_m \rangle = \sum_{\alpha\beta} \langle AE_\alpha | c_{l,\alpha} c_{m,\beta} | AE_\beta \rangle = \sum_{\alpha} c_{l,\alpha} c_{m,\alpha}. \tag{4}$$

The chemical identity of the central atom in each AE is retained, and only environments for the same chemical species are compared. The overall comparison is a linear combination of the individual comparisons:

$$\langle \phi_l | \phi_m \rangle = \sum_j \langle \phi_l | \phi_m \rangle_j n_j, \tag{5}$$

where n_j are fractions of each species at $\{X\}$.

The function describing the structural similarity between a metastable state, ϕ_l, and the ground state, ϕ^{gs}, is constructed to be a maximum when the pseudostructures have no AEs in common and zero when they are equivalent:

$$f(|\phi_l\rangle) = |1 - \langle \phi_l | \phi^{gs} \rangle| w_l, \tag{6}$$

where w_l is the weight of each pair (triplet) contributing to the GFA. They follow a Gaussian distribution based on the dimensionless difference between the local and global stoichiometries, $r_{i,l}$:

$$r_{i,l} = |\{x\}_i - \{X\}_l|, \quad R_l = \sum_i r_{i,l} b_{l,i}, \qquad w_l = \exp\left(\frac{-R_l^2}{2\sigma_R^2}\right), \tag{7}$$

and σ_R is a fitting factor set to 0.1. The average structural similarity amongst pairs (triplets) of metastable states, $\overline{ss}$, is calculated as:

$$\overline{ss} = \frac{\sum_{lm} (1 - \langle \phi_l | \phi_m \rangle) w_l w_m}{\sum_{lm} w_l w_m}. \tag{8}$$

The GFA computed for each stoichiometry of a given alloy system is normalized by the sum of the weights of each contribution, $\sum_l w_l$.

The function describing the enthalpy proximity between a metastable state and the ground state is:

$$g(H_l) = \exp\left(\frac{-|H_l - H^{gs}|}{k_B T_{room}}\right), \tag{9}$$

where H_l is the formation enthalpy per atom of a pseudostructure, H^{gs} is the formation enthalpy per atom of the ground state, and $k_B T_{room} = 25$ meV/atom ($T_{room} \sim 290$ K).

Finally, the overall GFA at each global stoichiometry $\{X\}$ is calculated as:

$$\chi_{GFA}(\{X\}) = \frac{100 \overline{ss}^2 \sum_l f(|\phi_l\rangle) g(H_l)}{\sum_l w_l}, \tag{10}$$

where 100 is an arbitrary scaling factor.

2.2. First-principles calculations of alloy prototypes

The crystal structures and formation enthalpies of the alloys are taken from the AFLOW.org repository [31–33]. The original calculations were performed systematically using the AFLOW computational materials design framework [36–38] and density functional theory as implemented in VASP [39,40]. AFLOW standard settings [41] were used: GGA-PBE exchange-correlation functional [42], PAW potentials [43,44], at least 6,000 k-points per reciprocal atom, and a plane-wave cutoff of at least 1.4 times the largest recommended value for the VASP potentials of the constituents. The input crystal structures were built from the AFLOW library of common prototypes [45,46].

2.3. Calculation of elastic properties

The elastic properties of metallic glasses have been extensively reviewed and can be estimated from the rule of mixtures [47,48]. Here, the following equation is used:

$$M^{-1} = \sum_j f_j M_j^{-1}, \tag{11}$$

where M is the elastic constant of the system, and f_j and M_j are the molar fraction and elastic constant of the component elements in bulk form. The elastic properties for the elements are taken from Ref. [49]. This method generally under-predicts the bulk modulus and over-predicts the shear modulus, K and G, respectively. Performing a linear regression on data for the 18 binary and ternary systems available in Ref. [47] that are relevant to the current study gives the equations:

$$K_{measured} = 1.12 K_{mixing} - 4.68, \quad R^2 = 0.97; \tag{12}$$

$$G_{measured} = 0.80 G_{mixing} + 2.92, \quad R^2 = 0.93. \tag{13}$$

Poisson's ratio, ν, is used to determine whether an alloy will be tough or brittle, as metallic glasses with $\nu < 0.34$ tend to exhibit brittle behavior [20,47]. Since metallic glasses are macroscopically isotropic, Poisson's ratio is calculated as:

$$\nu_{calc} = \frac{3K - 2G}{2(3K + G)}. \tag{14}$$

Using the $K_{measured}$ and $G_{measured}$ calculated from Eqns. (12) and (13) in Eqn. (14) correlates well with the measured Poisson's ratios reported in Ref. [47]:

$$\nu_{measured} = 1.10 \nu_{calc} - 0.04, \quad R^2 = 0.80. \tag{15}$$

Another commonly applied indicator of brittle *vs.* tough behavior, the Pugh's modulus ratio, G/K, is less reliably predicted from Eqns. (11)–(13). The Young's modulus, E, correlates with fracture strength, σ_f, as $\sigma_f = E/50$, and E is calculated as $E = 2.61G$ [47].

3. Results and discussion

3.1. GFA model validation

GFA predictions for five binary alloy systems known to form bulk metallic glasses are shown in Fig. 2. The cutoff energy for including crystal structures in the analysis of each system was chosen to represent a typical glass transition temperature for that system: 50 meV/atom (~580 K) for Al-Ca, 65 meV/atom (~750 K) for Cu-Hf and Cu-Zr, 80 meV/atom (~925 K) for Nb-Ni and 55 meV/atom (~640 K) for Pd-Si [50]. The compositions where glasses have been produced with a critical diameter greater than 1 mm [51–58] are also marked. In all cases, GFA greater than 1/3 of the system maximum is predicted at or near the experimentally determined bulk glass-forming compositions. The predictions made using the method in Ref. [30] are shown for comparison. Here, the cutoff energy was set to 50 meV/atom for all systems. Calculations with the current method were also performed at 50 meV/atom for all five systems, and only minor differences in the predictions resulted from the change. In some instances, there is a significant difference between the GFA calculated with the computational method in Ref. [30] *vs.* the present method, which can be attributed to the change in reference state. These are highlighted in Fig. 3 for Al-Ca and Pd-Si. At each highlighted composition a large GFA is calculated with the method in Ref. [30], which uses the structure with the lowest enthalpy of formation at a given stoichiometry for the reference state. Because the convex hull indicates a phase separation at these compositions, using it to find the reference state reduces the GFA. Other improvements to the predictions can be attributed to including contributions from local off-stoichiometry clusters, and to a lesser extent, changes in the comparison of the AEs. Precision is also increased by using the current model, since the GFA can be determined at compositions where no structures are available in the database.

GFA predictions for the known bulk glass-forming systems — Al-Cu-Zr [59–62], Al-Ni-Zr [63,74], Ca-Cu-Mg [64–66], Ca-Mg-Zn [67–71], and Cu-Mg-Y [72,73] — are shown in Fig. 4. The cutoff energy is set to 60 meV/atom (~700 K) for the Al-Cu-Zr and Al-Ni-Zr systems, and 35 meV/atom (~400 K) for the Ca-Cu-Mg, Ca-Mg-Zn, and Cu-Mg-Y systems. To reduce calculation time, a cutoff of $r_{i,l} = 3\sigma_R$ is imposed for including a pseudostructure in the GFA calculation, which was validated on the Ca-Cu-Mg, Ca-Mg-Zn, and Cu-Mg-Y systems. Regions where bulk glasses have been produced tend to be near compositions where high GFA is predicted, and additional compositions may be possible (Fig. 4). Experimentally, regions of potential bulk-glass formation in the Al-Ni-Zr system have been predicted by evaluating the supercooled liquid [74] and are outlined in purple. Reports emphasize that GFA changes rapidly with composition [72], and as little as 1% change in composition could change a result from amorphous to crystalline [59]. Therefore, it is important to comprehensively search the phase space. A broad search is performed computationally, revealing high GFA compositions far from experimentally confirmed glasses. These compositions offer a guide for experimentalists, but are limited in precision due to the sampling grid and available crystal structures.

Although differences between the predictions and experimental data could be due to lack of experimental reports at particular compositions, they may also result from physical phenomena not included in the model. The possibility for crystal nucleation and growth is partially captured by the comparison of AEs; however, diffusion kinetics are not taken into account. Comparisons of the packing densities of the available crystal structures, which relate to the ability of ions to diffuse [26,27,55], will be investigated in future extensions of the model.

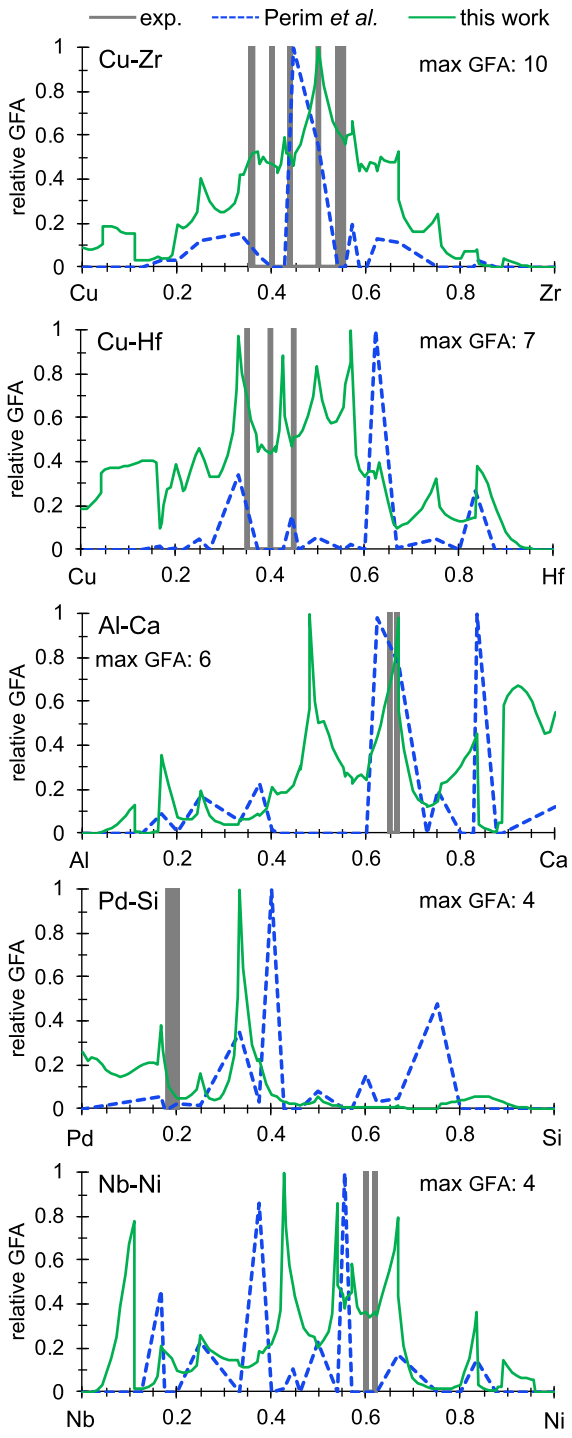

Fig. 2. GFA predictions for known bulk binary glass-forming systems. Predictions made using the method in Ref. [30] (dotted lines) and compositions where bulk alloys (critical diameter > 1 mm) were experimentally produced (vertical bars) are shown for comparison. The scale is relative to the maximum calculated GFA of the system. Experimental data was taken from Refs. [52,54,55] for Cu-Zr, [52,53] for Cu-Hf, [51] for Al-Ca, [58] for Pd-Si, and [56,57] for Nb-Ni.

3.2. Application to biologically relevant systems

Alloy systems based on macronutrient Mg and Ca are considered for orthopedic applications. Trace metals in the human body (Ba, Be, Co, Cr, Cu, Fe, Li, Mn, Mo, Ni, Sr, W, Zn), and antibacterial Ag [4,6,75] are included in smaller amounts. Although many of the

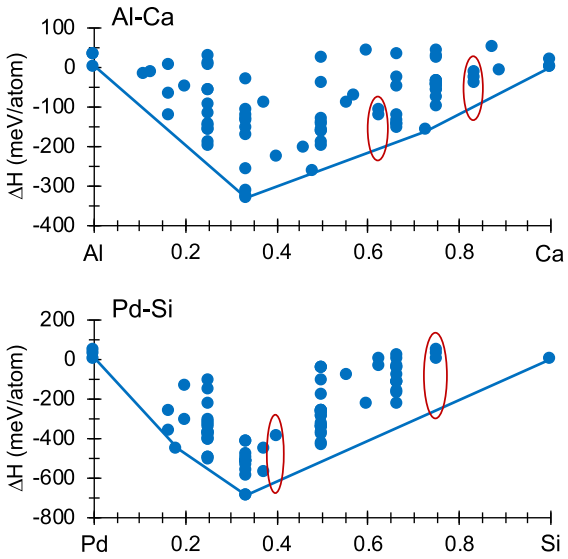

Fig. 3. Convex hull plots for known bulk glass-forming systems. Red ovals indicate compositions where using the convex hull to find the reference state for the GFA calculations significantly reduced the GFA. (For interpretation of the references to colour in this figure legend, the reader is referred to the Web version of this article.)

trace elements are known to be toxic at high concentrations [6], several are essential (*e.g.* Cu, Fe) or potentially beneficial (*e.g.* Li, Sr) for bone growth and function [4,76]. Therefore, the dosage via degradation rate and metabolic pathways of the elements warrant serious consideration in the design of biodegradable implant materials, which is beyond the scope of this study. The GFA for binary combinations of these 16 elements was calculated with a cutoff energy of 35 meV/atom, which corresponds to an expected $T_g \sim$ 400 K for Mg- and Ca-based systems [50]. Sampling for the binary systems ranges from 134 to 910 converged crystal structures. Upon removal of duplicates (one converged structure is equivalent to another converged structure [77,78]), structures with formation enthalpies greater than 35 meV/atom, and structures for which AEs could not be determined; 4 to 521 structures remain for each system for calculation of the GFA. Finally, systems with less than 20 remaining structures are considered to have insufficient sampling and removed from the analysis. This leaves 54 systems, of which 42 have a maximum GFA > 4.26 (the smallest maximum for known binary bulk glass-forming systems) and 20 have a maximum GFA > 10.06 (the largest maximum for known binary bulk glass-forming systems). The maximum GFA and the composition at which it occurs for these systems is shown in Fig. 5a. Metallic glasses have been produced experimentally for eight of them — Ag-Ca [79], Ca-Cu [79], Ca-Mg [79], Ca-Zn [79], Cu-Mg [80], Mg-Sr [79], Mg-Zn [81], and Sr-Zn [79].

The ternary system Cu-Mg-Zn is also studied. The glass transition temperature is assumed to be similar to the T_g of other Mg-based systems, therefore the energy cutoff is set to 35 meV/atom. Sampling for the ternary systems ranges from 1279 to 1582 converged crystal structures. Upon removal of duplicates, structures with formation enthalpies greater than the cutoff energy, and structures for which AEs could not be determined; 411 to 584 structures remain for each system for calculation of the GFA. The predictions are shown in Fig. 4. Cu-Mg-Zn has a maximum predicted GFA of 6, which is greater than the smallest maximum GFA for known bulk glass-forming systems; therefore it is expected to be a bulk glass-forming system.

GFA peaks greater than 1/3 of the system maximum for Mg-rich and Ca-rich binary alloys are presented in Table 1. The Young's moduli and Poisson's ratios for these alloy systems are plotted in Fig. 6, and the Young's moduli and Poisson's ratios for the best glass-forming compositions of the relevant ternary alloy systems — Ca-Cu-Mg, Ca-Mg-Zn, and Cu-Mg-Zn — are given in Table 2.

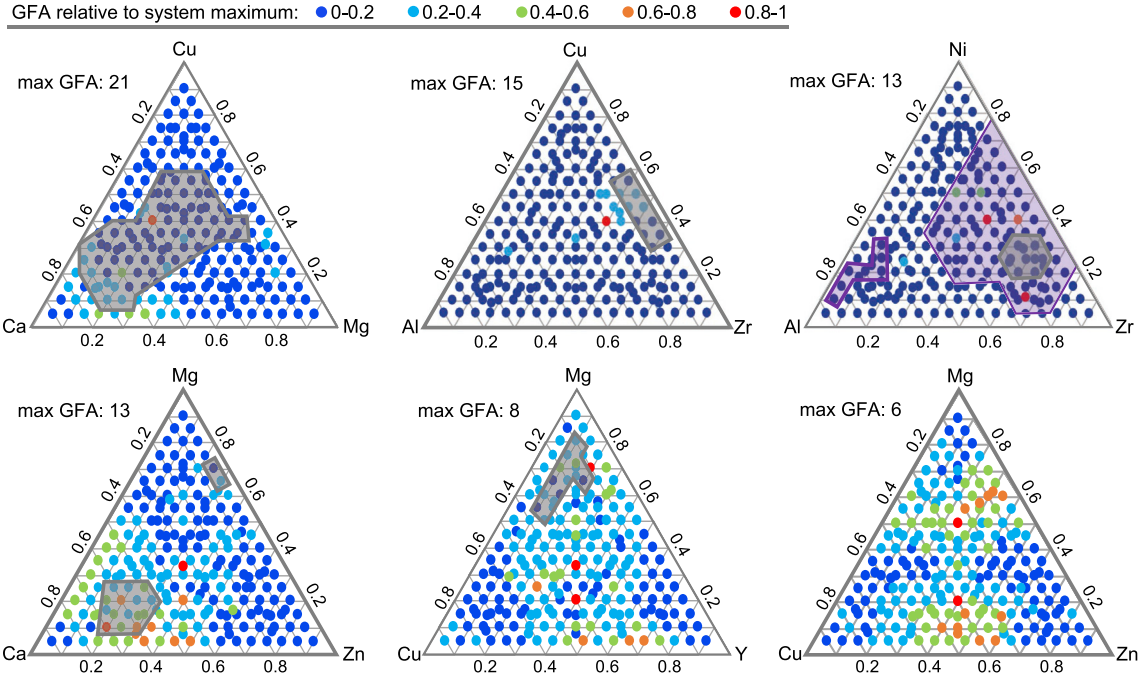

Fig. 4. GFA predictions for bulk ternary glass-forming systems. The GFA predictions for Ca-Cu-Mg, Al-Cu-Zr, Al-Ni-Zr, Ca-Mg-Zn, Cu-Mg-Y, and Cu-Mg-Zn systems are shown as circles; and approximate regions where bulk glasses have been produced are enclosed in grey shapes [59–73]. The purple shapes in the Al-Ni-Zr plot indicate regions of potential bulk glass-formation based on evaluation of the supercooled liquid [74]. (For interpretation of the references to colour in this figure legend, the reader is referred to the Web version of this article.)

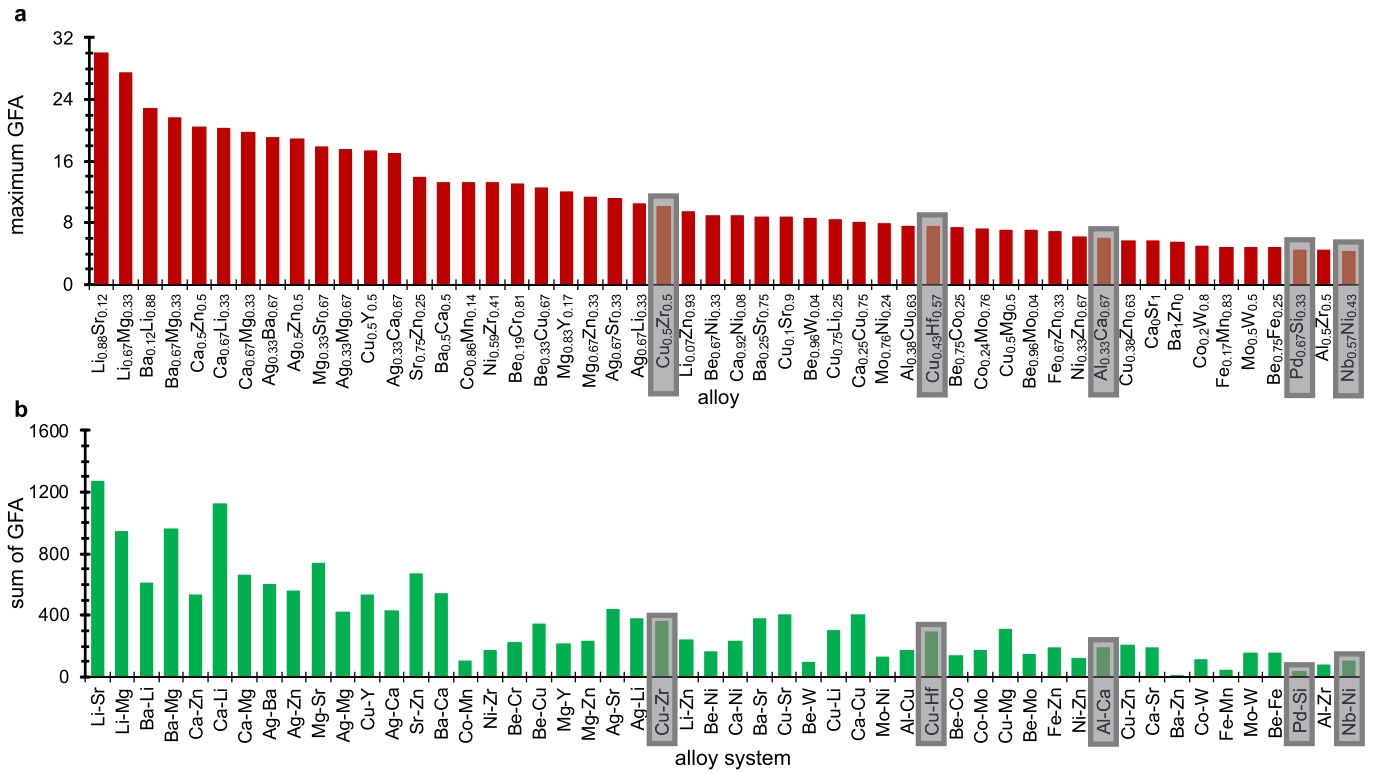

Fig. 5. GFA ranking of biologically relevant binary alloy systems: (**a**) system maximum and (**b**) sum of GFA. Known bulk glass-forming systems (enclosed in grey rectangles) and systems relevant to the ternary validation systems are shown for comparison.

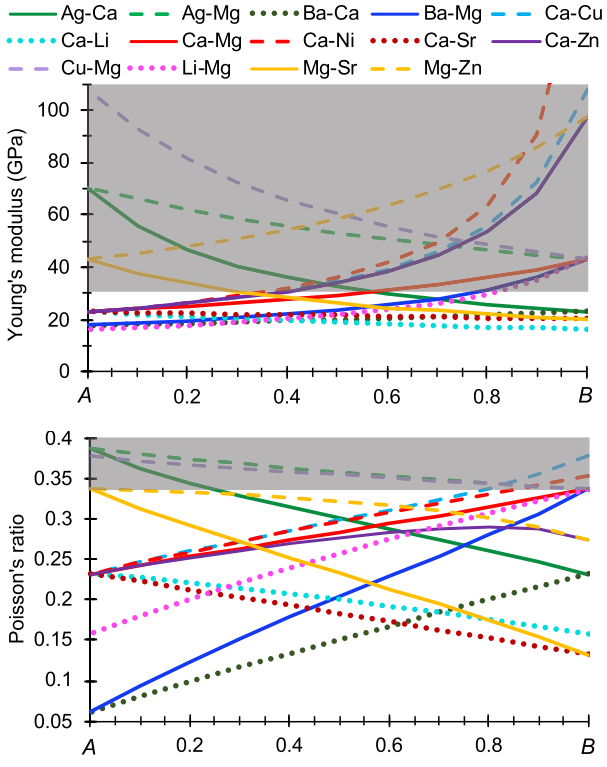

Fig. 6. Elastic properties of biologically relevant binary alloy systems. The Young's moduli and Poisson's ratios for *A-B* binary alloy systems are determined from the linear regression of experimental data with the rule of mixtures. See text for details. The grey regions indicate Young's moduli greater than bone [11] and expected high fracture toughness.

Many of the glasses presented in Tables 1 and 2 will be strong enough for orthopedic applications, as the Young's modulus of bone ranges from 3 to 30 GPa [11]. Stress shielding and tissue resorption can occur if the modulus of the implant is substantially higher than that of bone [16]. In these cases, engineering strategies such as forming a porous foam can be applied to reduce the modulus of the implant [82,83]. However, most of the alloys analyzed in this study are predicted to be brittle. This is not surprising, considering that the Poisson's ratio of pure elemental Ca is 0.31 and Mg is 0.29 [49]; and many of the Ca- and Mg-based metallic glasses studied experimentally exhibit brittle behavior [84–86]. Furthermore, Ca can develop a partially occupied *d*-shell when combined with Mg and other metals [87] leading to directional bonding, which may contribute to the brittle behavior of its compounds [88]. Some glasses have shown bending ductility in ribbon form after production, but embrittle at room-temperature after only a few days or weeks [81,86]. Researchers have suggested alloying with elements that minimize charge transfer [85,86] and directional bonding [88] to increase ductility, and elements with higher melting temperatures to increase stability [86]. We suggest alloys with high predicted Poisson's ratios.

Following the analyses of GFA and elastic properties, $Ag_{0.37}Mg_{0.63}$, $Ag_{0.33}Mg_{0.67}$, $Cu_{0.5}Mg_{0.5}$, $Cu_{0.37}Mg_{0.63}$, $Cu_{0.33}Mg_{0.67}$, and $Cu_{0.25}Mg_{0.5}Zn_{0.25}$ alloys are predicted to have high GFA, strength, and fracture toughness. Therefore, these alloys are recommended for further consideration as orthopedic support materials. Corrosion rate studies will be of particular interest to determine if the release rates of Cu and Ag ions are appropriate for biomedical implant applications. Additional ternary systems are suggested based on the results of the binary system GFA calculation and estimation of elastic properties.

The sum of the predicted GFA values for the six ternary systems correlate linearly with the sum of the GFAs in their component

Table 1
Ca- and Mg-rich peaks in biologically relevant binary systems with a predicted GFA at least 1/3 of the system maximum.

Alloy	Relative GFA	Alloy	Relative GFA
$Ag_{0.33}Ca_{0.67}$	1	$Ca_{0.5}Ni_{0.5}$	0.55
$Ag_{0.37}Ca_{0.63}$	0.51	$Ca_{0.92}Ni_{0.08}$	1
Ag_nCa_{1-n}, $0.05 < n < 0.14$	0.33–0.37	Ca_1Sr_0	0.58
$Ag_{0.37}Mg_{0.63}$	0.75	$Ca_{0.75}Sr_{0.25}$	0.62
$Ag_{0.33}Mg_{0.67}$	1	$Ca_{0.67}Sr_{0.33}$	0.43
$Ag_{0.25}Mg_{0.75}$	0.46	$Ca_{0.57}Sr_{0.43}$	0.68
$Ag_{0.2}Mg_{0.8}$	0.38	$Ca_{0.5}Sr_{0.5}$	0.62
Ag_nMg_{1-n}, $0.02 < n < 0.12$	0.34–0.4	$Ca_{0.65}Zn_{0.35}$	0.69
$Ba_{0.5}Ca_{0.5}$	1	$Ca_{0.5}Zn_{0.5}$	1
$Ba_{0.33}Ca_{0.67}$	0.73	$Cu_{0.5}Mg_{0.5}$	1
$Ba_{0.5}Mg_{0.5}$	0.68	$Cu_{0.37}Mg_{0.63}$	0.97
$Ba_{0.17}Mg_{0.83}$	0.63	$Cu_{0.33}Mg_{0.67}$	0.96
$Ca_{0.84}Cu_{0.16}$	0.99	$Cu_{0.25}Mg_{0.75}$	0.45
$Ca_{0.75}Cu_{0.25}$	0.95	Cu_nMg_{1-n}, $0 < n < 0.16$	0.39–0.52
Ca_nCu_{1-n}, $0.59 < n < 0.67$	0.54–0.56	Li_nMg_{1-n}, $0.33 < n < 0.5$	0.45–0.56
$Ca_{0.84}Li_{0.16}$	0.8	Mg_nSr_{1-n}, $0.9 < n < 0.98$	0.35–0.42
$Ca_{0.75}Li_{0.25}$	0.83	$Mg_{0.83}Sr_{0.17}$	0.53
$Ca_{0.67}Li_{0.33}$	1	$Mg_{0.5}Sr_{0.5}$	0.63
$Ca_{0.5}Li_{0.5}$	0.77	$Mg_{0.75}Zn_{0.25}$	0.4
$Ca_{0.5}Mg_{0.5}$	0.71	$Mg_{0.67}Zn_{0.33}$	1
$Ca_{0.57}Mg_{0.43}$	0.62	$Mg_{0.5}Zn_{0.5}$	0.4
$Ca_{0.67}Mg_{0.33}$	1		

Table 2
GFA, Young's modulus (E), and Poisson's ratio (ν) for Ca-Cu-Mg, Ca-Mg-Zn, and Cu-Mg-Zn compositions where the GFA is greater than 60% of the system maximum. The Young's moduli and Poisson's ratios are determined from the linear regression of experimental data with the rule of mixtures. See text for details.

Alloy	GFA	E (GPa)	ν
$Ca_{0.4}Cu_{0.4}Mg_{0.2}$	21	36	0.31
$Ca_{0.7}Mg_{0.1}Zn_{0.2}$	13	28	0.26
$Ca_{0.33}Mg_{0.33}Zn_{0.33}$	10	37	0.30
$Ca_{0.6}Mg_{0.2}Zn_{0.2}$	10	29	0.27
$Ca_{0.6}Mg_{0.1}Zn_{0.3}$	10	30	0.27
$Ca_{0.6}Mg_{0.05}Zn_{0.35}$	9	30	0.27
$Ca_{0.62}Mg_{0.08}Zn_{0.31}$	9	30	0.27
$Ca_{0.5}Mg_{0.05}Zn_{0.45}$	8	33	0.28
$Ca_{0.4}Mg_{0.2}Zn_{0.4}$	8	36	0.29
$Ca_{0.55}Mg_{0.1}Zn_{0.35}$	8	31	0.27
$Ca_{0.45}Mg_{0.05}Zn_{0.5}$	8	35	0.28
$Cu_{0.4}Mg_{0.2}Zn_{0.4}$	6	79	0.33
$Cu_{0.25}Mg_{0.5}Zn_{0.25}$	5	59	0.34
$Cu_{0.08}Mg_{0.62}Zn_{0.31}$	5	54	0.33
$Cu_{0.35}Mg_{0.05}Zn_{0.6}$	5	94	0.31
$Cu_{0.1}Mg_{0.6}Zn_{0.3}$	5	55	0.33
$Cu_{0.4}Mg_{0.05}Zn_{0.55}$	5	95	0.32
$Cu_{0.14}Mg_{0.57}Zn_{0.29}$	4	56	0.33
$Cu_{0.45}Mg_{0.1}Zn_{0.45}$	4	89	0.33
$Cu_{0.29}Mg_{0.14}Zn_{0.57}$	4	83	0.32
$Cu_{0.05}Mg_{0.6}Zn_{0.35}$	4	55	0.33
$Cu_{0.4}Mg_{0.15}Zn_{0.45}$	4	83	0.33
$Cu_{0.2}Mg_{0.55}Zn_{0.25}$	4	57	0.34
$Cu_{0.5}Mg_{0.1}Zn_{0.4}$	4	89	0.33
$Cu_{0.46}Mg_{0.08}Zn_{0.46}$	4	92	0.33

binary systems. Since the sum of the GFA for a system comprises the aspects of maximum and breadth, it is used as a rough indicator of potential good higher-order glass-forming systems. Considering ternary systems which can be created from the set {Ag, Ba, Be, Ca, Co, Cr, Cu, Fe, Li, Mg, Mn, Mo, Ni, Sr, W, Zn}, include Ca and/or Mg, and include only binary pairs with sufficient sampling and GFA > 4.26; there are 30 additional potential glass-forming systems available for further analysis. Including the six validation systems, the rank of GFA sum from best to worst is {Li-Mg-Sr, Ca-Li-Mg, Ca-Li-Sr, Ba-Li-Mg, Ba-Ca-Li, Ba-Ca-Mg, Ba-Mg-Sr, Ag-Ba-Mg, Ag-Ca-Li, Ca-Li-Zn, Ca-Cu-Li, Ag-Li-Mg, Mg-Sr-Zn, Ag-Mg-Sr, Ca-Mg-Sr, Ag-Ba-Ca, Cu-Li-Mg, Ag-Ca-Zn, Ag-Ca-Mg, Cu-Mg-Sr, Ca-Mg-Zn, Li-Mg-Zn, Ca-Sr-Zn, Ca-Cu-Mg, Ag-Mg-Zn, Ba-Mg-Zn, Ca-Cu-Zn, Ba-Ca-Sr, Ba-Ca-Zn, Cu-Mg-Y, Ag-Ca-Sr, Ca-Cu-Sr, Ca-Ni-Zn, Cu-Mg-Zn, Al-Cu-Zr, Al-Ni-Zr}. The GFA sums for their component binary systems are given in Fig. 5b.

Estimations of Poisson's ratios indicate that mostly Ag-rich alloys will fall into the tough regime, although some Mg-rich alloys in the Ag-Ca-Mg and Ag-Mg-Zn systems have an estimated Poisson's ratio greater than 0.33 and Young's modulus greater than 30 GPa. Toughness in these alloys is further promoted by the full d-shells in Ag and Zn [88]. Some experimental work has been performed for Ag addition to Ca- and Mg-based alloys. Partial substitution of Ag for Cu in $Cu_{0.25}Mg_{0.65}Y_{0.1}$ increased the GFA [89], and substitution of 1–3% Ag for Zn in $Ca_{0.04}Mg_{0.66}Zn_{0.3}$ decreased the GFA but increased the corrosion resistance [90]. A wide composition range of Ag-Ca-Mg bulk metallic glasses have been produced [65,88,91]. Based on these promising theoretical and experimental results, we suggest further exploration of Ag-Ca-Mg and Ag-Mg-Zn alloy systems.

4. Conclusions

A model to predict the glass-forming ability (GFA) of binary and ternary alloys systems was developed based on the competition between crystalline phases, and implemented in the AFLOW framework. The model was applied to material systems relevant for biodegradable orthopedic support implants. Alloys predicted to have high GFA were further analyzed for elastic properties based on the rule of mixtures. Alloys predicted to have high GFA, a Young's modulus at least as high as bone's, and high fracture toughness based on the Poisson's ratio include: $Ag_{0.33}Mg_{0.67}$, $Cu_{0.5}Mg_{0.5}$, $Cu_{0.37}Mg_{0.63}$ and $Cu_{0.25}Mg_{0.5}Zn_{0.25}$. Finally, the GFA of binary systems was correlated with the GFA of ternary systems. Based on this and the analysis of elastic properties, the Ag-Ca-Mg and Ag-Mg-Zn systems are recommended for further study.

Research data

All of the *ab-initio* alloy data is freely available to the public as part of the AFLOW online repository and can be accessed through www.aflow.org following the REST-API interface [32] and the AFLUX search language [92].

Acknowledgements

We thank Dr. Jan Schroers and Dr. Sungwoo Sohn for discussions. This work was supported by the National Science Foundation under DMREF Grant No. DMR-1436151; and DOD-ONR under Grants No. N00014-17-1-2090, N00014-13-1-0635, and N00014-16-1-2326. D.C.F. acknowledges support from the Duke University Provost's Postdoctoral Fellowship Program. D.H. acknowledges support from the Department of Defense through the National Defense Science and Engineering Graduate (NDSEG) Fellowship Program. C.O. acknowledges support from the National Science Foundation Graduate Research Fellowship under Grant No. DGF1106401.

Appendix A. Supplementary data

Supplementary data to this article can be found online at https://doi.org/10.1016/j.actamat.2019.07.008.

References

[1] W.L. Johnson, Bulk glass-forming metallic alloys: science and technology, MRS Bull. 24 (10) (1999) 42–56, https://doi.org/10.1557/S0883769400053252.
[2] J.J. Kruzic, Bulk metallic glasses as structural materials: a review, Adv. Eng. Mater. 18 (2016) 1308–1331, https://doi.org/10.1002/adem.201600066.
[3] H.F. Li, Y.F. Zheng, Recent advances in bulk metallic glasses for biomedical applications, Acta Biomater. 36 (2016) 1–20, https://doi.org/10.1016/j.actbio.2016.03.047.
[4] G. Kaur, O.P. Pandey, K. Singh, D. Homa, B. Scott, G. Pickrell, A review of bioactive glasses: their structure, properties, fabrication, and apatite formation, J. Biomed. Mater. Res. A 102A (2014) 254–274, https://doi.org/10.1002/jbm.a.34690.
[5] C. Suryanarayana, A. Inoue, Iron-based bulk metallic glasses, Int. Mater. Rev. 58 (2013) 131–166, https://doi.org/10.1179/1743280412Y.0000000007.
[6] Q. Chen, G.A. Thouas, Metallic implant biomaterials, Math. Sci. Eng. R 87 (2015) 1–57, https://doi.org/10.1016/j.mser.2014.10.001.
[7] M.P. Staiger, A.M. Pietak, J. Huadmai, G. Dias, Magnesium and its alloys as orthopedic biomaterials: a review, Biomaterials 27 (2006) 1728–1734, https://doi.org/10.1016/j.biomaterials.2005.10.003.
[8] J. Walker, S. Shadanbaz, T.B.F. Woodfield, M.P. Staiger, G.J. Dias, Magnesium biomaterials for orthopedic application: a review from a biological perspective, J. Biomed. Mater. Res. Part B 102B (2014) 1316–1331, https://doi.org/10.1002/jbm.b.33113.
[9] K.F. Farraro, K.E. Kim, S.L.-Y. Woo, J.R. Flowers, M.B. McCullough, Revolutionizing orthopaedic biomaterials: the potential of biodegradable and bioresorbable magnesium-based materials for functional tissue engineering, J. Biomech. 47 (2014) 1979–1986, https://doi.org/10.1016/j.jbiomech.2013.12.003.
[10] Y. Chen, Z. Xu, C. Smith, J. Sankar, Recent advances on the development of magnesium alloys for biodegradable implants, Acta Biomater. 10 (2014) 4561–4573, https://doi.org/10.1016/j.actbio.2014.07.005.
[11] S. Jafari, S.E. Harandi, R.K.S. Raman, A review of stress-corrosion cracking and corrosion fatigue of magnesium alloys for biodegradable implant applications, JOM 67 (2015) 1143–1153, https://doi.org/10.1007/s11837-015-1366-z.
[12] S. Agarwal, J. Curtin, B. Duffy, S. Jaiswal, Biodegradable magnesium alloys for orthopaedic applications: a review on corrosion, biocompatibility and surface modifications, Mater. Sci. Eng. C 68 (2016) 948–963, https://doi.org/10.1016/j.msec.2016.06.020.
[13] T.S.N.S. Narayanan, I.S. Park, M.H. Lee, Strategies to improve the corrosion resistance of microarc oxidation (MAO) coated magnesium alloys for degradable implants: prospects and challenges, Prog. Mater. Sci. 60 (2014) 1–71, https://doi.org/10.1016/j.pmatsci.2013.08.002.
[14] T. Kraus, S.F. Fischerauer, A.C. Hänzi, P.J. Uggowitzer, J.F. Löffler, A.M. Weinberg, Magnesium alloys for temporary implants in osteosynthesis: in vivo studies of their degradation and interaction with bone, Acta Biomater. 8 (2012) 1230–1238, https://doi.org/10.1016/j.actbio.2011.11.008.
[15] G. Song, Control of biodegradation of biocompatable magnesium alloys, Corros. Sci. 49 (2007) 1696–1701, https://doi.org/10.1016/j.corsci.2007.01.001.
[16] H. Ibrahim, S.N. Esfahani, B. Poorganji, D. Dean, M. Elahinia, Resorbable bone fixation alloys, forming, and post-fabrication treatments, Mater. Sci. Eng. C 70 (2017) 870–888, https://doi.org/10.1016/j.msec.2016.09.069.
[17] Y.Q. Cheng, E. Ma, Atomic-level structure and structure-property relationship in metallic glasses, Prog. Mater. Sci. 56 (2011) 379–473, https://doi.org/10.1016/j.pmatsci.2010.12.002.
[18] J.R. Scully, A. Gebert, J.H. Payer, Corrosion and related mechanical properties of bulk metallic glasses, J. Mater. Res. 22 (2007) 302–313, https://doi.org/10.1557/JMR.2007.0051.
[19] B. Zberg, P.J. Uggowitzer, J.F. Löffler, MgZnCa glasses without clinically observable hydrogen evolution for biodegradable implants, Nat. Mater. 8 (2009) 887–891, https://doi.org/10.1038/NMAT2542.
[20] J.J. Lewandowski, W.H. Wang, A.L. Greer, Intrinsic plasticity or brittleness of metallic glasses, Phil. Mag. Lett. 85 (2005) 77–87, https://doi.org/10.1080/09500830500080474.
[21] M. Chen, Mechanical behavior of metallic glasses: microscopic understanding of strength and ductility, Annu. Rev. Mater. Res. 38 (2008) 445–469, https://doi.org/10.1146/annurev.matsci.38.060407.130226.
[22] A. Inoue, Stabilization of metallic supercooled liquid and bulk amorphous alloys, Acta Mater. 48 (1) (2000) 279–306, https://doi.org/10.1016/S1359-6454(99)00300-6.
[23] Y. Li, S. Zhao, Y. Liu, P. Gong, J. Schroers, How many bulk metallic glasses are there? ACS Comb. Sci. 19 (2017) 687–693, https://doi.org/10.1021/acscombsci.7b00048.
[24] F. Ren, L. Ward, T. Williams, K.J. Laws, C. Wolverton, J. Hattrick-Simpers, A. Mehta, Accelerated discovery of metallic glasses through iteration of machine learning and high-throughput experiments, Sci. Adv. 4 (2018), eaaq1566, https://doi.org/10.1126/sciadv.aaq1566.
[25] S. Vincent, D.R. Peshwe, B.S. Murty, J. Bhatt, Thermodynamic prediction of bulk metallic glass forming alloys in ternary Zr-Cu-*X* (*X* = Ag, Al, Ti, Ga) systems, J. Non-Cryst. Solids 357 (2011) 3495–3499, https://doi.org/10.1016/j.jnoncrysol.2011.06.024.
[26] K.J. Laws, D.B. Miracle, M. Ferry, A predictive structural model for bulk metallic glasses, Nat. Commun. 6 (2015) 8123, https://doi.org/10.1038/ncomms9123.
[27] K. Zhang, B. Dice, Y. Liu, J. Schroers, M.D. Shattuck, C.S. O'Hern, On the origin of multi-component bulk metallic glasses: atomic size mismatches and demixing, J. Chem. Phys. 143 (5) (2015), 054501, https://doi.org/10.1063/1.4927560.
[28] D.V. Louzguine-Luzgin, D.B. Miracle, L. Louzguina-Luzgina, A. Inoue, Comparative analysis of glass-formation in binary, ternary, and multicomponent alloys, J. Appl. Phys. 108 (2010) 103511, https://doi.org/10.1063/1.3506687.
[29] A.L. Greer, Confusion by design, Nature 366 (6453) (1993) 303–304, https://doi.org/10.1038/366303a0.
[30] E. Perim, D. Lee, Y. Liu, C. Toher, P. Gong, Y. Li, W.N. Simmons, O. Levy, J.J. Vlassak, J. Schroers, S. Curtarolo, Spectral descriptors for bulk metallic glasses based on the thermodynamics of competing crystalline phases, Nat. Commun. 7 (2016) 12315, https://doi.org/10.1038/ncomms12315.
[31] W. Setyawan, S. Curtarolo, AFLOWLIB: Ab-Initio Electronic Structure Library Database, 2011. http://www.aflow.org.
[32] R.H. Taylor, F. Rose, C. Toher, O. Levy, K. Yang, M. Buongiorno Nardelli, S. Curtarolo, A RESTful API for exchanging materials data in the AFLOWLIB.org consortium, Comput. Mater. Sci. 93 (2014) 178–192, https://doi.org/10.1016/j.commatsci.2014.05.014.
[33] S. Curtarolo, W. Setyawan, S. Wang, J. Xue, K. Yang, R.H. Taylor, L.J. Nelson, G.L.W. Hart, S. Sanvito, M. Buongiorno Nardelli, N. Mingo, O. Levy, AFLOWLIB.ORG: a distributed materials properties repository from high-throughput *ab initio* calculations, Comput. Mater. Sci. 58 (2012) 227–235, https://doi.org/10.1016/j.commatsci.2012.02.002.
[34] P. Villars, Factors governing crystal structures, in: J.H. Westbrook, R.L. Fleischer (Eds.), Crystal Structures of Intermetallic Compounds, Wiley, New York, 2000, pp. 1–49.
[35] C. Oses, E. Gossett, D. Hicks, F. Rose, M.J. Mehl, E. Perim, I. Takeuchi, S. Sanvito, M. Scheffler, Y. Lederer, O. Levy, C. Toher, S. Curtarolo, AFLOW-CHULL: cloud-oriented platform for autonomous phase stability analysis, J. Chem. Inf. Model. 58 (12) (2018) 2477–2490, https://doi.org/10.1021/acs.jcim.8b00393.
[36] C. Toher, et al., The AFLOW fleet for materials discovery, in: W. Andreoni, S. Yip (Eds.), Handbook of Materials Modeling, Springer International Publishing, Cham, Switzerland, 2018, pp. 1–28, https://doi.org/10.1007/978-3-319-42913-7_63-1.
[37] C. Oses, C. Toher, S. Curtarolo, Data-driven design of inorganic materials with the automatic flow framework for materials discovery, MRS Bull. 43 (2018) 670–675, https://doi.org/10.1557/mrs.2018.207.
[38] S. Curtarolo, W. Setyawan, G.L.W. Hart, M. Jahnátek, R.V. Chepulskii, R.H. Taylor, S. Wang, J. Xue, K. Yang, O. Levy, M.J. Mehl, H.T. Stokes, D.O. Demchenko, D. Morgan, AFLOW: an automatic framework for high-throughput materials discovery, Comput. Mater. Sci. 58 (2012) 218–226, https://doi.org/10.1016/j.commatsci.2012.02.005.
[39] G. Kresse, J. Hafner, *Ab initio* molecular dynamics for liquid metals, Phys. Rev. B 47 (1993) 558–561, https://doi.org/10.1103/PhysRevB.47.558.
[40] G. Kresse, J. Furthmüller, Efficient iterative schemes for *ab initio* total-energy calculations using a plane-wave basis set, Phys. Rev. B 54 (1996) 11169–11186, https://doi.org/10.1103/PhysRevB.54.11169.
[41] C.E. Calderon, J.J. Plata, C. Toher, C. Oses, O. Levy, M. Fornari, A. Natan, M.J. Mehl, G.L.W. Hart, M. Buongiorno Nardelli, S. Curtarolo, The AFLOW standard for high-throughput materials science calculations, Comput. Mater. Sci. 108 (Part A) (2015) 233–238, https://doi.org/10.1016/j.commatsci.2015.07.019.
[42] J.P. Perdew, K. Burke, M. Ernzerhof, Generalized gradient approximation made simple, Phys. Rev. Lett. 77 (1996) 3865–3868, https://doi.org/10.1103/PhysRevLett.77.3865.
[43] P.E. Blöchl, Projector augmented-wave method, Phys. Rev. B 50 (1994) 17953–17979, https://doi.org/10.1103/PhysRevB.50.17953.
[44] G. Kresse, D. Joubert, From ultrasoft pseudopotentials to the projector augmented-wave method, Phys. Rev. B 59 (1999) 1758–1775, https://doi.org/

10.1103/PhysRevB.59.1758.
[45] M.J. Mehl, D. Hicks, C. Toher, O. Levy, R.M. Hanson, G.L.W. Hart, S. Curtarolo, The AFLOW library of crystallographic prototypes: Part 1, Comput, Mater. Sci. 136 (2017) S1–S828, https://doi.org/10.1016/j.commatsci.2017.01.017.
[46] D. Hicks, M.J. Mehl, E. Gossett, C. Toher, O. Levy, R.M. Hanson, G.L.W. Hart, S. Curtarolo, The AFLOW library of crystallographic prototypes: Part 2, Comput, Mater. Sci. 161 (2019) S1–S1011, https://doi.org/10.1016/j.commatsci.2018.10.043.
[47] W.H. Wang, The elastic properties, elastic models and elastic perspectives of metallic glasses, Prog. Mater. Sci. 57 (2012) 487–656, https://doi.org/10.1016/j.pmatsci.2011.07.001.
[48] Y. Zhang, A.L. Greer, Correlations for predicting plasticity or brittleness of metallic glasses, J. Alloy. Comp. 434–435 (2007) 2–5, https://doi.org/10.1016/j.jallcom.2006.08.094.
[49] WebElements, The Periodic Table of the Elements. https://www.webelements.com.
[50] D.B. Miracle, D.V. Louzguine-Luzgin, L.V. Louzguina-Luzgina, A. Inoue, An assessment of binary metallic glasses: correlations between structure, glass forming ability and stability, Int. Mater. Rev. 55 (2010) 218–256, https://doi.org/10.1179/095066010X12646898728200.
[51] F.Q. Guo, S.J. Poon, G.J. Shiflet, CaAl-based bulk metallic glasses with high thermal stability, Appl. Phys. Lett. 84 (2004) 37–39, https://doi.org/10.1063/1.1637940.
[52] A. Inoue, W. Zhang, Formation, thermal stability and mechanical properties of Cu-Zr and Cu-Hf binary glassy alloy rods, Mater. Trans. 45 (2) (2004) 584–587, https://doi.org/10.2320/matertrans.45.584.
[53] L. Xia, D. Ding, S.T. Shan, Y.D. Dong, The glass forming ability of Cu-rich Cu-Hf binary alloys, J. Phys. Condens. Matter 18 (15) (2006) 3543, https://doi.org/10.1088/0953-8984/18/15/002.
[54] D. Wang, Y. Li, B.B. Sun, M.L. Sui, K. Lu, E. Ma, Bulk metallic glass formation in the binary Cu-Zr system, Appl. Phys. Lett. 84 (20) (2004) 4029–4031, https://doi.org/10.1063/1.1751219.
[55] Y. Li, Q. Guo, J.A. Kalb, C.V. Thompson, Matching glass-forming ability with the density of the amorphous phase, Science 322 (5909) (2008) 1816–1819, https://doi.org/10.1126/science.1163062.
[56] L. Xia, W.H. Li, S.S. Fang, B.C. Wei, Y.D. Dong, Binary Ni-Nb bulk metallic glasses, J. Appl. Phys. 99 (2006), 026103, https://doi.org/10.1063/1.2158130.
[57] M. Leonhardt, W. Löser, H.-G. Lindenkreuz, Solidification kinetics and phase formation of undercooled eutectic Ni-Nb melts, Acta Mater. 47 (10) (1999) 2961–2968, https://doi.org/10.1016/S1359-6454(99)00167-6.
[58] H.S. Chen, D. Turnbull, Formation, stability, and structure of palladium-silicon based alloy glasses, Acta Metall. 17 (1969) 1021–1031, https://doi.org/10.1016/0001-6160(69)90048-0.
[59] D. Wang, H. Tan, Y. Li, Multiple maxima of GFA in three adjacent eutectics in Zr-Cu-Al alloy system — a metallographic way to pinpoint the best glass forming alloys, Acta Mater. 53 (2005) 2969–2979, https://doi.org/10.1016/j.actamat.2005.03.012.
[60] Y.C. Kim, J.C. Lee, P.R. Cha, J.P. Ahn, E. Fleury, Enhanced glass forming ability and mechanical properties of new Cu-based bulk metallic glasses, Mater. Sci. Eng. A 437 (2006) 248–253, https://doi.org/10.1016/j.msea.2006.07.141.
[61] D.H. Xu, G. Duan, W.L. Johnson, Unusual glass-forming ability of bulk amorphous alloys based on ordinary metal copper, Phys. Rev. Lett. 92 (2004) 245504, https://doi.org/10.1103/PhysRevLett.92.245504.
[62] A. Inoue, High strength bulk amorphous alloys with low critical cooling rates, Mater. Trans. 36 (1995) 866–875, https://doi.org/10.2320/matertrans1989.36.866.
[63] Y.H. Li, W. Zhang, C. Dong, J.B. Qiang, G.Q. Xie, K. Fujita, A. Inoue, Glass-forming ability and corrosion resistance of Zr-based Zr-Ni-Al bulk metallic glasses, J. Alloy. Comp. 536S (2012) S117–S121, https://doi.org/10.1016/j.jallcom.2011.11.073.
[64] O.N. Senkov, J.M. Scott, D.B. Miracle, Composition range and glass forming ability of ternary Ca-Mg-Cu bulk metallic glasses, J. Alloy. Comp. 424 (2006) 394–399, https://doi.org/10.1016/j.jallcom.2006.01.104.
[65] K.J. Laws, K.F. Shamlaye, J.D. Cao, J.P. Scicluna, M. Ferry, Locating new Mg-based bulk metallic glasses free of rare earth elements, J. Alloy. Comp. 542 (2012) 105–110, https://doi.org/10.1016/j.jallcom.2012.07.028.
[66] K.J. Laws, K.F. Shamlaye, K. Wong, B. Gun, M. Ferry, Prediction of glass-forming compositions in metallic systems: copper-based bulk metallic glasses in the Cu-Mg-Ca system, Metall. Mater. Trans. A 41A (2010) 1699–1705, https://doi.org/10.1007/s11661-010-0274-7.
[67] K.J. Laws, K.F. Shamlaye, B. Gun, K. Wong, M. Ferry, The prediction of glass-forming compositions in metallic systems – the development of new bulk metallic glasses, Mater. Sci. Forum 638–642 (2010) 1637–1641, https://doi.org/10.4028/www.scientific.net/MSF.638-642.1637.
[68] J.D. Cao, N.T. Kirkland, K.J. Laws, N. Birbilis, M. Ferry, Ca-Mg-Zn bulk metallic glasses as bioresorbable metals, Acta Biomater. 8 (2012) 2375–2383, https://doi.org/10.1016/j.actbio.2012.03.009.
[69] X. Gu, G.J. Shiflet, F.Q. Guo, S.J. Poon, Mg-Ca-Zn bulk metallic glasses with high strength and significant ductility, J. Mater. Res. 20 (2005) 1935–1938, https://doi.org/10.1557/JMR.2005.0245.
[70] O.N. Senkov, J.M. Scott, Glass forming ability and thermal stability of ternary Ca-Mg-Zn bulk metallic glasses, J. Non-Cryst. Solids 351 (2005) 3087–3094, https://doi.org/10.1016/j.jnoncrysol.2005.07.022.
[71] E.S. Park, D.H. Kim, Formation of Ca-Mg-Zn bulk glassy alloy by casting into cone-shaped copper mold, J. Mater. Res. 19 (2004) 685–688, https://doi.org/10.1557/jmr.2004.19.3.685.
[72] H. Ma, Q. Zheng, J. Xu, Y. Li, E. Ma, Doubling the critical size for bulk metallic glass formation in the Mg-Cu-Y ternary system, J. Mater. Res. 20 (2005) 2252–2255, https://doi.org/10.1557/jmr.2005.0307.
[73] A. Inoue, A. Kato, T. Zhang, S.G. Kim, T. Masumoto, Mg-Cu-Y amorphous alloys with high mechanical strengths produced by a metallic mold casting method, Mater. Trans. 32 (1991) 609–616, https://doi.org/10.2320/matertrans1989.32.609.
[74] A. Inoue, T. Zhang, T. Masumoto, Zr-Al-Ni amorphous alloys with high glass transition temperature and significant supercooled liquid region, Mater. Trans. 31 (1990) 177–183, https://doi.org/10.2320/matertrans1989.31.177.
[75] D.M. Vasconcelos, S.G. Santos, M. Lamghari, M.A. Barbosa, The two faces of metal ions: from implants rejection to tissue repair/regeneration, Biomaterials 84 (2016) 262–275, https://doi.org/10.1016/j.biomaterials.2016.01.046.
[76] M. Dermience, G. Lognay, F. Mathieu, P. Goyens, Effects of thirty elements on bone metabolism, J. Trace Elem. Med. Biol. 32 (2015) 86–106, https://doi.org/10.1016/j.jtemb.2015.06.005.
[77] D. Hicks, C. Oses, E. Gossett, G. Gomez, R.H. Taylor, C. Toher, M.J. Mehl, O. Levy, S. Curtarolo, *AFLOW-SYM*: platform for the complete, automatic and self-consistent symmetry analysis of crystals, Acta Crystallogr. A 74 (3) (2018) 184–203, https://doi.org/10.1107/S2053273318003066.
[78] D. Hicks, C. Toher, D. C. Ford, F. Rose, C. De Santo, O. Levy, M. J. Mehl, S. Curtarolo, AFLOW-XTAL-MATCH: Automated Method for Quantifying the Structural Similarity of Materials and Identifying Unique Crystal Prototypes, (in preparation).
[79] R.S. Amand, B.C. Giessen, Easy glass formation in simple metal alloys: amorphous metals containing calcium and strontium, Scr. Metall. 12 (1978) 1021–1026, https://doi.org/10.1016/0036-9748(78)90017-0.
[80] S.G. Kim, A. Inoue, T. Masumoto, High mechanical strengths of Mg-Ni-Y and Mg-Cu-Y amorphous alloys with significant supercooled liquid region, Mater. Trans. 31 (1990) 929–934, https://doi.org/10.2320/matertrans1989.31.929.
[81] A. Calka, M. Madhava, D.E. Polk, B.C. Giessen, H. Matyja, J. Vander Sande, A transition-metal-free amorphous alloy: $Mg_{.70}Zn_{.30}$, Scr. Metall. 11 (1977) 65–70, https://doi.org/10.1016/0036-9748(77)90015-1.
[82] G. Ryan, A. Pandit, D.P. Apatsidis, Fabrication methods of porous metals for use in orthopaedic applications, Biomaterials 27 (2006) 2651–2670, https://doi.org/10.1016/j.biomaterials.2005.12.002.
[83] P. Meagher, E.D. O'Cearbhaill, J.H. Byrne, D.J. Browne, Bulk metallic glasses for implantable medical devices and surgical tools, Adv. Mater. 28 (2016) 5755–5762, https://doi.org/10.1002/adma.201505347.
[84] F. Guo, S.J. Poon, X. Gu, G.J. Shiflet, Low-density Mg-rich metallic glasses with bending ductility, Scr. Mater. 56 (2007) 689–692, https://doi.org/10.1016/j.scriptamat.2006.12.028.
[85] M. Widom, B. Sauerwine, A.M. Cheung, S.J. Poon, P. Tong, D. Louca, G.J. Shiflet, Elastic properties of Ca-based metallic glasses predicted by first-principles simulations, Phys. Rev. B 84 (2011), 054206, https://doi.org/10.1103/PhysRevB.84.054206.
[86] K.J. Laws, D. Granata, J.F. Löffler, Alloy design strategies for sustained ductility in Mg-based amorphous alloys — tackling structural relaxation, Acta Mater. 103 (2016) 735–745, https://doi.org/10.1016/j.actamat.2015.08.077.
[87] Z.-S. Mo, M.-X. Zeng, R.-N. Wang, X.-J. Chen, B.-Y. Tang, L.-M. Peng, W.-J. Ding, Study of the structural, elastic and electronic properties of ordered $Ca(Mg_{1-x}Li_x)_2$ alloys from first-principles calculations, Phys. Scripta 84 (2011), 055603, https://doi.org/10.1088/0031-8949/84/05/055603.
[88] K.J. Laws, K.F. Shamlaye, D. Granata, L.S. Koloadin, J.F. Löffler, Electron-band theory inspired design of magnesium-precious metal bulk metallic glasses with high thermal stability and extended ductility, Sci. Rep. 7 (2017) 3400, https://doi.org/10.1038/s41598-017-03643-7.
[89] E.S. Park, H.G. Kang, W.T. Kim, D.H. Kim, The effect of Ag addition on the glass-forming ability of Mg-Cu-Y metallic glass alloys, J. Non-Cryst. Solids 279 (2001) 154–160, https://doi.org/10.1016/S0022-3093(00)00412-9.
[90] H. Li, S. Pang, Y. Liu, P.K. Liaw, T. Zhang, In vitro investigation of Mg-Zn-Ca-Ag bulk metallic glasses for biomedical applications, J. Non-Cryst. Solids 427 (2015) 134–138, https://doi.org/10.1016/j.jnoncrysol.2015.07.043.
[91] K. Amiya, A. Inoue, Formation and thermal stability of Ca-Mg-Ag-Cu bulk glassy alloys, Mater. Trans. 43 (2002) 2578–2581, https://doi.org/10.2320/matertrans.43.2578.
[92] F. Rose, C. Toher, E. Gossett, C. Oses, M. Buongiorno Nardelli, M. Fornari, S. Curtarolo, AFLUX: the LUX materials search API for the AFLOW data repositories, Comput. Mater. Sci. 137 (2017) 362–370, https://doi.org/10.1016/j.commatsci.2017.04.036.